Title

Construction of G2 rounded corners with Pythagorean-hodograph curves

Journal

Computer Aided Geometric Design, 31(2)

ISSN

0167-8396

Author

Farouki, Rida T

Publication Date

2014-02-01

DOI

10.1016/j.cagd.2014.02.002

Peer reviewed

Construction of G^2 rounded corners with Pythagorean–hodograph curves

Rida T. Farouki
Department of Mechanical and Aerospace Engineering,
University of California, Davis, CA 95616, USA.

Abstract

The problem of designing smoothly rounded right–angle corners with Pythagorean–hodograph (PH) curves is addressed. A G^1 corner can be uniquely specified as a single PH cubic segment, closely approximating a circular arc. Similarly, a G^2 corner can be uniquely constructed with a single PH quintic segment having a unimodal curvature distribution. To obtain G^2 corners incorporating shape freedoms that permit a fine tuning of the curvature profile, PH curves of degree 7 are required. It is shown that degree 7 PH curves define a one–parameter family of G^2 corners, facilitating precise control over the extremum of the unimodal curvature distribution, within a certain range of the parameter. As an alternative, a G^2 corner construction based upon splicing together two PH quintic segments is proposed, that provides two free parameters for shape adjustment. The smooth corner shapes constructed through these schemes can exploit the computational advantages of PH curves, including exact computation of arc length, rational offset curves, and real–time interpolator algorithms for motion control in manufacturing, robotics, inspection, and similar applications.

Keywords: rounded corners; Pythagorean–hodograph curves; complex polynomials; G^2 continuity; curvature distribution.

e–mail: farouki@ucdavis.edu

1 Introduction

The problem of "smoothly rounding" the sharp corners of a nominal shape is a key requirement in many geometric design contexts. In consumer products or architectural design, for example, rounded corners are often preferred on the basis of aesthetic or ergonomic considerations. The rounding or "filleting" of sharp corners in load–bearing mechanical components plays a critical role in minimizing stress concentration effects, and thus prolonging fatigue life. In the layout of highways or railways, the precise variation of curvature along a turn between linear segments determines the maximum safe traversal speed, due to the instantaneous centripetal acceleration it incurs.

The focus of this study is on the design of G^2 corner shapes with planar Pythagorean–hodograph (PH) curves, a family of curves compatible with the standard Bézier/B–spline representations of modern CAD systems, that offer attractive computational advantages over "ordinary" polynomial curves [4]. Despite its ubiquitous applications, this "corner rounding" problem does not appear to have received much attention. Walton and Meek [19] formulated a scheme for G^2 blending of the corners on polygonal curves using "ordinary" cubic and PH quintic segments. The unique G^2 PH quintic corner described in Section 4 below may be regarded as a special case of this scheme, but it offers no residual degrees freedoms for fine–tuning the corner shape.

A substantial literature on design of "spiral segments" has accumulated [1, 7, 8, 9, 10, 11, 12, 13] including the use of PH curves [3, 6, 14, 15, 16, 17, 18, 20] in this context. However, spiral segments are not directly applicable to the corner rounding problem, since they have monotone curvature variation, and a G^2 rounded corner shape must incorporate vanishing end–point curvatures. It is, in principle, possible to construct a G^2 rounded corner shape by splicing spiral PH curve segments together.[1] But a single–segment solution, which is G^∞ over its interior, is obviously preferable whenever possible.

The solution procedure (and the analysis of the existence of solutions) is much simpler if the PH curve corner–rounding problem is addressed directly, rather than as an application of existing spiral–segment methods. Invoking the complex representation of planar PH curves, it is shown that G^2 rounded corners with the desired symmetry and unimodal curvature properties can be constructed using little more than the solutions of quadratic equations. For brevity, the focus of this study is on rounding right–angle corners (the case of

[1] Such a solution is presented in Section 6 below.

most practical importance). However, the methods can be extended without undue complication to the case of corners with acute or obtuse angles.

The plan for the remainder of this paper is as follows. Section 2 briefly reviews the construction and basic properties of planar PH curves, and their advantageous features in the corner rounding problem. The simplest solution, the G^1 PH cubic corner, is then derived in Section 3, and is found to be unique and to closely approximate a circular arc. Quintic PH curves are necessary to obtain a G^2 corner, and in Section 4 it is observed that the G^2 PH quintic corner is also unique, with a unimodal curvature distribution. Proceeding to degree 7 PH curves in Section 5, a G^2 corner incorporating one free parameter is constructed. The curvature remains unimodal over a certain range of this parameter, which can be exploited to fine tune the extremum curvature. As an alternative, another G^2 scheme based on splicing together two PH quintic curves is described in Section 6, that provides two free parameters for shape adjustment. Finally, Section 7 summarizes the main results of this study and identifies some possible topics for further investigation.

2 Planar Pythagorean–hodograph curves

A planar polynomial Pythagorean–hodograph (PH) curve $\mathbf{r}(\xi) = (x(\xi), y(\xi))$ is characterized by the fact that its derivative components $x'(\xi), y'(\xi)$ satisfy [5] the Pythagorean condition

$$x'^2(\xi) + y'^2(\xi) \;=\; \sigma^2(\xi) \tag{1}$$

for some polynomial $\sigma(\xi)$, which defines the *parametric speed* of $\mathbf{r}(\xi)$, i.e., the rate of change $\mathrm{d}s/\mathrm{d}\xi$ of arc length s with repect to the curve parameter ξ. The fact that $\sigma(\xi)$ is a polynomial (rather than the square root of a polynomial) endows PH curves with several attractive computational properties.

For a primitive curve — i.e., $\gcd(x'(\xi), y'(\xi)) = \text{constant}$ — a sufficient and necessary condition for satisfaction of (1) is that $x'(\xi)$ and $y'(\xi)$ should be expressible in terms of polynomials $u(\xi)$, $v(\xi)$ in the form

$$x'(\xi) \;=\; u^2(\xi) - v^2(\xi)\,, \quad y'(\xi) \;=\; 2\,u(\xi)v(\xi)\,.$$

This structure is captured by the complex representation [2], in which a PH curve of degree $n = 2m+1$ is generated from a degree–m complex polynomial

$$\mathbf{w}(\xi) \;=\; u(\xi) + \mathrm{i}\,v(\xi) \;=\; \sum_{k=0}^{m} \mathbf{w}_k \binom{m}{k} (1-\xi)^{m-k}\xi^k \tag{2}$$

with Bernstein coefficients $\mathbf{w}_k = u_k + \mathrm{i}\, v_k$ by integration of the expression

$$\mathbf{r}'(\xi) \;=\; \mathbf{w}^2(\xi)\,. \tag{3}$$

The parametric speed, unit tangent, and curvature of $\mathbf{r}(\xi)$ may be formulated [2] in terms of $\mathbf{w}(\xi)$ as

$$\sigma(\xi) \;=\; |\mathbf{w}(\xi)|^2\,, \quad \mathbf{t}(\xi) \;=\; \frac{\mathbf{w}^2(\xi)}{\sigma(\xi)}\,, \quad \kappa(\xi) \;=\; 2\,\frac{\mathrm{Im}(\overline{\mathbf{w}}(\xi)\mathbf{w}'(\xi))}{\sigma^2(\xi)}\,. \tag{4}$$

As noted above, the parametric speed is a polynomial, while the unit tangent and curvature[2] are rational functions of ξ. The unit normal $\mathbf{n}(\xi) = \mathbf{t}(\xi) \times \mathbf{z}$, where $\mathbf{z}$ is a unit vector orthogonal to the plane, is also rational. Since $\sigma(\xi)$ is a polynomial, the cumulative arc length

$$s(\xi) \;=\; \int_0^{\xi} \sigma(t)\; \mathrm{d}t$$

is also a polynomial in ξ. Moreover, the offset curves

$$\mathbf{r}_d(\xi) \;=\; \mathbf{r}(\xi) \;+\; d\,\mathbf{n}(\xi)$$

at each distance d can be exactly represented as rational curves.

To construct smooth PH curve corner shapes, it is convenient to adopt a standardized coordinate system. Solutions obtained in this system can be transformed to specific model coordinates through a suitable combination of scaling, translation, and rotation transformations. A *canonical G^2 corner* is defined as a smooth curve, with initial and final positions, unit tangents, and curvatures specified by

$$\mathbf{p}_i = (0,0), \quad \mathbf{t}_i = (1,0), \quad \kappa_i = 0, \qquad \mathbf{p}_f = (1,1), \quad \mathbf{t}_f = (0,1), \quad \kappa_f = 0\,.$$

Furthermore, the corner curve should exhibit monotone variation of its x, y coordinates between the end points, a unimodal curvature distribution, and be symmetric about the diagonal line from $(0,1)$ to $(1,0)$. If the curvature conditions $\kappa_i = \kappa_f = 0$ are relaxed, we have a *canonical G^1 corner*.

[2]The numerator and denominator of $\kappa(\xi)$ are of degree $2m-2$ and $4m$, respectively.

3 Unique G^1 PH cubic corner

The simplest non–trivial planar PH curves are cubics. PH cubics are capable of (uniquely) defining a canonical G^1 corner, but not a G^2 corner. Any PH cubic is simply a translated, rotated, scaled and re–parameterized segment of a unique curve — the *Tschirnhaus cubic* [5]. Instead of using the complex representation, the PH cubics may be characterized by simple geometrical constraints on their Bézier control polygons, namely

$$L_2 \;=\; \sqrt{L_1 L_3} \qquad \text{and} \qquad \theta_1 \;=\; \theta_2 \,, \tag{5}$$

where L_1, L_2, L_3 are the lengths of the control polygon legs, and θ_1, θ_2 are the interior control polygon angles. Writing

$$\mathbf{r}(\xi) \;=\; \mathbf{p}_0(1-\xi)^3 + \mathbf{p}_1 3(1-\xi)^2\xi + \mathbf{p}_2 3(1-\xi)\xi^2 + \mathbf{p}_3\xi^3 \,,$$

one can easily verify that the unique PH cubic with $\mathbf{r}(0) = \mathbf{p}_i$, $\mathbf{r}(1) = \mathbf{p}_f$ and $\mathbf{r}'(0) = |\mathbf{r}'(0)|\,\mathbf{t}_i$, $\mathbf{r}'(1) = |\mathbf{r}'(1)|\,\mathbf{t}_f$ has the control points

$$\mathbf{p}_0 = (0,0)\,, \quad \mathbf{p}_1 = (2-\sqrt{2},0)\,, \quad \mathbf{p}_2 = (1,\sqrt{2}-1)\,, \quad \mathbf{p}_3 = (1,1)\,,$$

and satisfies conditions (5) with $L_1 = L_2 = L_3 = 2-\sqrt{2}$ and $\theta_1 = \theta_2 = \frac{3}{4}\pi$. The parametric speed of this curve is specified by the quadratic polynomial

$$\sigma(\xi) \;=\; |\mathbf{r}'(\xi)| \;=\; \sigma_0(1-\xi)^2 + \sigma_1 2(1-\xi)\xi + \sigma_2\xi^2$$

with coefficients $\sigma_0 = \sigma_2 = 3(2-\sqrt{2})$ and $\sigma_1 = 3(\sqrt{2}-1)$. It has a rather mild variation between $3(2-\sqrt{2}) \approx 1.757359$ at the end–points and 1.5 at the mid–point, $\mathbf{r}(\frac{1}{2}) = \frac{1}{8}(10-3\sqrt{2}, 3\sqrt{2}-2) \approx (0.719670, 0.280330)$.

The total arc length of the G^1 PH cubic corner is $S = \frac{1}{3}(\sigma_0+\sigma_1+\sigma_2) = 3-\sqrt{2} \approx 1.585786$ ($\sim 12.1\%$ greater than the chord length). The curvature can be expressed as

$$\kappa(\xi) \;=\; \frac{6(\sqrt{2}-1)}{\sigma^2(\xi)}\,,$$

and it increases from $\kappa(0) = \kappa(1) = (1+\sqrt{2})/3 \approx 0.804738$ at the end points to $\kappa(\frac{1}{2}) = 8(\sqrt{2}-1)/3 \approx 1.104570$ at the mid–point, an increase of $\sim 37\%$ (due entirely to the variation of the parametric speed).

As may be seen in Figure 1, the shape of the G^1 cubic corner curve is not aesthetically displeasing, and may be satisfactory for many design problems.

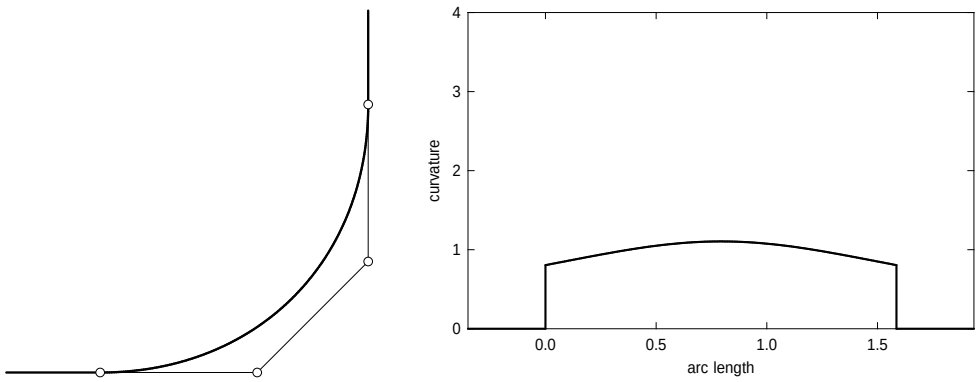

Figure 1: Left: canonical G^1 PH cubic corner curve, togther with its Bézier control polygon. Right: curvature profile of the G^1 PH cubic corner curve.

In fact, as seen in Figure 2, it closely approximates an arc of the unit circle. The greatest distance

$$d = \tfrac{1}{4}\sqrt{59 - 30\sqrt{2}} \approx 1.017767$$

from the center of the circle occurs at the mid–point $\mathbf{r}(\frac{1}{2})$, amounting to a deviation of $< 2\%$. The main drawback of the G^1 PH cubic is the curvature discontinuity it incurs in rounding out a right–angle corner (see Figure 1).

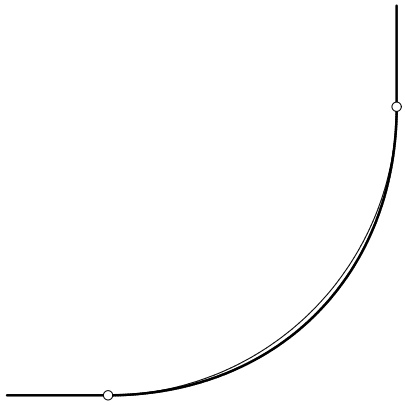

Figure 2: Comparison of G^1 PH cubic corner (bold curve) and a circular arc (light curve) — the maximum deviation from the circular arc is less than 2%.

4 Unique G^2 PH quintic corner

Since the cubic PH curves can only define G^1 corners (with no residual shape freedoms), we now consider the quintic PH curves. It is advantageous to use the complex representation defined by (2) and (3) with $m = 2$. Consider the PH quintic $\mathbf{r}(\xi)$ defined by subsituting a quadratic complex polynomial

$$\mathbf{w}(\xi) \;=\; \mathbf{w}_0(1-\xi)^2 + \mathbf{w}_1 2(1-\xi)\xi + \mathbf{w}_2\xi^2 \tag{6}$$

into (3) and integrating. The Bézier control points of $\mathbf{r}(\xi)$ may be determined from the coefficients $\mathbf{w}_0, \mathbf{w}_1, \mathbf{w}_2$ as

$$\begin{aligned}
\mathbf{p}_1 &= \mathbf{p}_0 + \frac{1}{5}\,\mathbf{w}_0^2\,,\\
\mathbf{p}_2 &= \mathbf{p}_1 + \frac{1}{5}\,\mathbf{w}_0\mathbf{w}_1\,,\\
\mathbf{p}_3 &= \mathbf{p}_2 + \frac{1}{5}\,\frac{2\mathbf{w}_1^2 + \mathbf{w}_0\mathbf{w}_2}{3}\,,\\
\mathbf{p}_4 &= \mathbf{p}_3 + \frac{1}{5}\,\mathbf{w}_1\mathbf{w}_2\,,\\
\mathbf{p}_5 &= \mathbf{p}_4 + \frac{1}{5}\,\mathbf{w}_2^2\,,
\end{aligned} \tag{7}$$

where $\mathbf{p}_0$ is a free integration constant. The end–derivatives of $\mathbf{r}(\xi)$ are

$$\mathbf{r}'(0) \;=\; \mathbf{w}_0^2 \qquad \text{and} \qquad \mathbf{r}'(1) \;=\; \mathbf{w}_2^2\,, \tag{8}$$

and its end–point curvatures of $\mathbf{r}(\xi)$ are specified by

$$\kappa(0) \;=\; 4\,\frac{\mathrm{Im}(\overline{\mathbf{w}}_0\mathbf{w}_1)}{|\mathbf{w}_0|^4} \qquad \text{and} \qquad \kappa(1) \;=\; 4\,\frac{\mathrm{Im}(\overline{\mathbf{w}}_1\mathbf{w}_2)}{|\mathbf{w}_2|^4}\,. \tag{9}$$

Symmetric interpolation of the end tangents and curvatures thus implies that $\mathbf{w}_0, \mathbf{w}_1, \mathbf{w}_2$ must satisfy

$$\mathbf{w}_0^2 \;=\; \lambda^2\,, \quad \mathbf{w}_2^2 \;=\; \mathrm{i}\,\lambda^2 \qquad \text{and} \qquad \mathrm{Im}(\overline{\mathbf{w}}_0\mathbf{w}_1) \;=\; \mathrm{Im}(\overline{\mathbf{w}}_1\mathbf{w}_2) \;=\; 0$$

for a non–zero real value λ. Since the curve defined by substituting $\mathbf{w}(\xi)$ into (3) and integrating is unchanged on replacing $\mathbf{w}_0, \mathbf{w}_1, \mathbf{w}_2$ by $-\mathbf{w}_0, -\mathbf{w}_1, -\mathbf{w}_2$ we may assume that

$$\mathbf{w}_0 \;=\; \lambda \;>\; 0 \tag{10}$$

from the first condition, while the second condition gives

$$\mathbf{w}_2 \;=\; s\frac{1+\mathrm{i}}{\sqrt{2}}\,\lambda\,, \tag{11}$$

where $s = \pm 1$. Writing $\mathbf{w}_1 = u_1 + \mathrm{i}\,v_1$ and substituting $\mathbf{w}_0, \mathbf{w}_2$ into the last two conditions then gives $v_1 = u_1 - v_1 = 0$, i.e., $\mathbf{w}_1 = 0$. From (7) we then have $\mathbf{p}_2 = \mathbf{p}_1$ and $\mathbf{p}_4 = \mathbf{p}_3$, so the G^2 corner is a special PH quintic, with just four distinct control points instead of six [2]. The fact that any PH quintic with zero end curvatures must have $\mathbf{w}_1 = 0$, and hence $\mathbf{p}_2 = \mathbf{p}_1$ and $\mathbf{p}_4 = \mathbf{p}_3$, has been noted (in a more general context) in Theorem 5.1 of [19].

With $\mathbf{p}_0 = 0$ and $\mathbf{p}_5 = 1 + \mathrm{i}$, interpolation of the corner end points yields the condition

$$\frac{1}{5}\left[\,\mathbf{w}_0^2 + \mathbf{w}_0\mathbf{w}_1 + \frac{2\mathbf{w}_1^2 + \mathbf{w}_0\mathbf{w}_2}{3} + \mathbf{w}_1\mathbf{w}_2 + \mathbf{w}_2^2\,\right] \;=\; 1 + \mathrm{i}\,,$$

and on substituting for $\mathbf{w}_0, \mathbf{w}_1, \mathbf{w}_2$ this becomes

$$\frac{1}{5}\left[\,\lambda^2 + s\frac{1+\mathrm{i}}{3\sqrt{2}}\,\lambda^2 + \mathrm{i}\,\lambda^2\,\right] \;=\; 1 + \mathrm{i}\,,$$

which is equivalent to

$$(3\sqrt{2} + s)\lambda^2 \;=\; 15\sqrt{2}\,.$$

Hence, since $\lambda > 0$ by assumption, we have

$$\lambda \;=\; \left[\frac{15\sqrt{2}}{3\sqrt{2}+s}\right]^{1/2}\,. \tag{12}$$

Although the sign choices $s = \pm 1$ both define formally correct interpolants to the prescribed data, only $s = +1$ generates an acceptable G^2 corner curve (see Figure 3). The curve defined by taking $s = -1$ exhibits negative curvature and a tight loop, so it must be discounted.

Hence, there exists an essentially unique canonical G^2 PH quintic corner, specified by the coefficients (10)–(12) with $s = 1$. Setting $c = 3(6 - \sqrt{2})/17$, the control points of this curve can be expressed as

$$\mathbf{p}_0 = (0,0)\,, \quad \mathbf{p}_1 = \mathbf{p}_2 = (c,0)\,, \quad \mathbf{p}_3 = \mathbf{p}_4 = (1, 1-c)\,, \quad \mathbf{p}_5 = (1,1)\,.$$

The canonical G^2 PH quintic corner may be regarded as a special case of the solution described in Section 5 of [19], corresponding to the choices $h = k = 1$

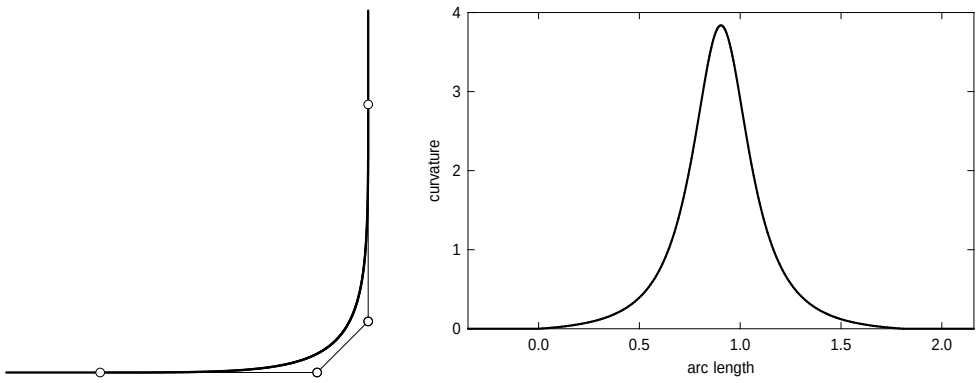

Figure 3: Left: canonical G^2 PH quintic corner curve, with its Bézier control polygon — note that, since $\mathbf{p}_1 = \mathbf{p}_2$ and $\mathbf{p}_3 = \mathbf{p}_4$, there are only four distinct control points. Right: curvature profile of the G^2 PH quintic corner curve.

and $\theta = \frac{1}{2}\pi$. The curvature profile is shown in Figure 3 — compared to the G^1 PH cubic corner in Figure 1, it is evident that the imposition of zero end curvatures incurs a much stronger variation of curvature.

The parametric speed is defined by the quadratic polynomial

$$\sigma(\xi) \;=\; \sum_{k=0}^{4} \sigma_k \binom{4}{k} (1-\xi)^{4-k} \xi^k$$

with coefficients

$$\sigma_0 = \sigma_4 = \frac{15}{17}(6-\sqrt{2})\,, \quad \sigma_1 = \sigma_3 = 0\,, \quad \sigma_2 = \frac{5}{17}(3\sqrt{2}-1)\,.$$

It varies from $15(6-\sqrt{2})/17 \approx 4.046282$ at the end points to $15(5+2\sqrt{2})/136 \approx 0.863429$ at the midpoint, namely

$$\mathbf{r}(\tfrac{1}{2}) \;=\; \frac{(542-45\sqrt{2},\, 2+45\sqrt{2})}{544} \;\approx\; (0.879339, 0.120661)\,.$$

The arc length of the G^2 PH quintic corner is $S = \frac{1}{5}(\sigma_0+\sigma_1+\sigma_2+\sigma_3+\sigma_4) = (35-3\sqrt{2})/17 \approx 1.809256$, or $\sim 27.9\%$ greater than the chord length. The curvature of this PH quintic can be expressed as

$$\kappa(\xi) \;=\; \frac{60}{17}(3\sqrt{2}-1)\frac{(1-\xi)\xi}{\sigma^2(\xi)}\,. \tag{13}$$

It increases from 0 at the end points to $\kappa(\frac{1}{2}) = 64(7\sqrt{2}-9)/15 \approx 3.837845$ at the mid–point. From Figure 3 one gains the impression that the G^2 PH quintic corner is almost G^3, i.e., the arc–length derivative of curvature $\mathrm{d}\kappa/\mathrm{d}s$ vanishes at its end points. From (13) one can verify it is not exactly G^3 since

$$\left.\frac{\mathrm{d}\kappa}{\mathrm{d}s}\right|_{\xi=0} = -\left.\frac{\mathrm{d}\kappa}{\mathrm{d}s}\right|_{\xi=1} = \frac{12+19\sqrt{2}}{225} \approx 0.172756\,.$$

5 Degree 7 G^2 PH corner

Since the G^2 PH quintic corner curve offers no residual shape freedoms, we consider now G^2 corners specified by degree 7 planar PH curves. Such curves are defined by substituting a cubic complex polynomial

$$\mathbf{w}(\xi) = \mathbf{w}_0(1-\xi)^3 + \mathbf{w}_1 3(1-\xi)^2\xi + \mathbf{w}_2 3(1-\xi)\xi^2 + \mathbf{w}_3\xi^3$$

into the hodograph (3) and integrating. For symmetric interpolation of the end tangents we must have $\mathbf{r}'(0) = \lambda^2$ and $\mathbf{r}'(1) = \mathrm{i}\,\lambda^2$ with $\lambda \neq 0$. Since $\mathbf{r}'(0) = \mathbf{w}_0^2$ and $\mathbf{r}'(1) = \mathbf{w}_3^2$, these conditions imply that

$$\mathbf{w}_0 = \lambda \quad \text{and} \quad \mathbf{w}_3 = p\frac{1+\mathrm{i}}{\sqrt{2}}\lambda\,, \tag{14}$$

where $p = \pm 1$ and we again take $\lambda > 0$ without loss of generality. Also, since

$$\kappa(0) = 6\,\frac{\mathrm{Im}(\overline{\mathbf{w}}_0\mathbf{w}_1)}{|\mathbf{w}_0|^4} \quad \text{and} \quad \kappa(1) = 6\,\frac{\mathrm{Im}(\overline{\mathbf{w}}_2\mathbf{w}_3)}{|\mathbf{w}_3|^4}\,,$$

the conditions $\kappa(0) = 0$ and $\kappa(1) = 0$, together with the symmetry constraint $|\mathbf{w}_1| = |\mathbf{w}_2|$, imply that

$$\mathbf{w}_1 = \mu \quad \text{and} \quad \mathbf{w}_2 = q\,\frac{1+\mathrm{i}}{\sqrt{2}}\mu \tag{15}$$

where $q = \pm 1$, for some real number μ. Finally, with $\mathbf{p}_0 = 0$ and $\mathbf{p}_3 = 1+\mathrm{i}$, the end–point displacement condition

$$\int_0^1 \mathbf{r}'(\xi)\,\mathrm{d}\xi = \mathbf{p}_3 - \mathbf{p}_0 = 1+\mathrm{i}$$

yields the equation

$$\frac{1}{7}\left[\,\mathbf{w}_0^2+\mathbf{w}_0\mathbf{w}_1+\frac{3\mathbf{w}_1^2+2\mathbf{w}_0\mathbf{w}_2}{5}+\frac{\mathbf{w}_0\mathbf{w}_3+9\mathbf{w}_1\mathbf{w}_2}{10}\right.$$
$$\left.+\,\frac{3\mathbf{w}_2^2+2\mathbf{w}_1\mathbf{w}_3}{5}+\mathbf{w}_2\mathbf{w}_3+\mathbf{w}_3^2\,\right]\;=\;1+\mathrm{i}\,.$$

Substituting for $\mathbf{w}_0,\mathbf{w}_1,\mathbf{w}_2,\mathbf{w}_3$, the real and imaginary parts of the above condition yield the two equations

$$(10\sqrt{2}+p)\,\lambda^2\;+\;2\,(5\sqrt{2}+2p+2q)\,\lambda\mu\;+\;(6\sqrt{2}+9q)\,\mu^2\;=\;70\sqrt{2}\,,$$
$$(10\sqrt{2}+p)\,\lambda^2\;+\;2\,(5\sqrt{2}\,pq+2p+2q)\,\lambda\mu\;+\;(6\sqrt{2}+9q)\,\mu^2\;=\;70\sqrt{2}\,,$$

for λ,μ. In order for these equations to be consistent, we must have $pq=1$, i.e., $p=q$, and the two equations are then identical. Setting

$$a=\frac{20+\sqrt{2}\,s}{140}\,,\quad b=\frac{10+4\sqrt{2}\,s}{140}\,,\quad c=\frac{12+9\sqrt{2}\,s}{140}\,,$$

where $s=\pm1$, they can be expressed in the form

$$\left[\begin{array}{cc}\lambda & \mu\end{array}\right]\left[\begin{array}{cc}a & b\\ b & c\end{array}\right]\left[\begin{array}{c}\lambda\\ \mu\end{array}\right]\;=\;1\,. \tag{16}$$

The eigenvalues of the 2×2 matrix are

$$\zeta_1,\zeta_2\;=\;\frac{a+c\pm\sqrt{(a-c)^2+4b^2}}{2}\;=\;\frac{16+5\sqrt{2}\,s\pm2\sqrt{45+12\sqrt{2}\,s}}{140}\,,$$

and the corresponding unit eigenvectors are

$$\frac{1}{\sqrt{(\zeta_1-a)^2+b^2}}\left[\begin{array}{c}b\\ \zeta_1-a\end{array}\right]\qquad\text{and}\qquad\frac{1}{\sqrt{(\zeta_2-a)^2+b^2}}\left[\begin{array}{c}b\\ \zeta_2-a\end{array}\right].$$

Assuming that $\zeta_1<\zeta_2$, both eigenvalues are positive when $s=+1$, but ζ_1 is negative and ζ_2 positive when $s=-1$.

By diagonalizing the matrix on the left in equation (16) its solutions may be parameterized in terms of a free angular variable ϕ when $s=+1$ as

$$\lambda(\phi)\;=\;\frac{b\cos\phi}{\sqrt{\zeta_1[\,(\zeta_1-a)^2+b^2\,]}}+\frac{b\sin\phi}{\sqrt{\zeta_2[\,(\zeta_2-a)^2+b^2\,]}}\,, \tag{17}$$
$$\mu(\phi)\;=\;\frac{(\zeta_1-a)\cos\phi}{\sqrt{\zeta_1[\,(\zeta_1-a)^2+b^2\,]}}+\frac{(\zeta_2-a)\sin\phi}{\sqrt{\zeta_2[\,(\zeta_2-a)^2+b^2\,]}}\,, \tag{18}$$

and when $s = -1$ as

$$\lambda(\phi) \;=\; \frac{b\tan\phi}{\sqrt{|\zeta_1|[\,(\zeta_1-a)^2+b^2\,]}} \;+\; \frac{b\sec\phi}{\sqrt{\zeta_2[\,(\zeta_2-a)^2+b^2\,]}}\,, \tag{19}$$

$$\mu(\phi) \;=\; \frac{(\zeta_1-a)\tan\phi}{\sqrt{|\zeta_1|[\,(\zeta_1-a)^2+b^2\,]}} \;+\; \frac{(\zeta_2-a)\sec\phi}{\sqrt{\zeta_2[\,(\zeta_2-a)^2+b^2\,]}}\,. \tag{20}$$

As shown in Figure 4, the above solutions describe an ellipse and a hyperbola, respectively, in the (λ, μ) plane. In practice, ϕ can be restricted to the interval $[\,0, \pi\,]$ in the case of (17)–(18), since it is apparent that replacing ϕ with $\phi+\pi$ simply reverses the sign of λ and μ, and hence also $\mathbf{w}_0, \mathbf{w}_1, \mathbf{w}_2, \mathbf{w}_3$ from (14) and (15), and such a sign reversal leaves the curve unchanged.

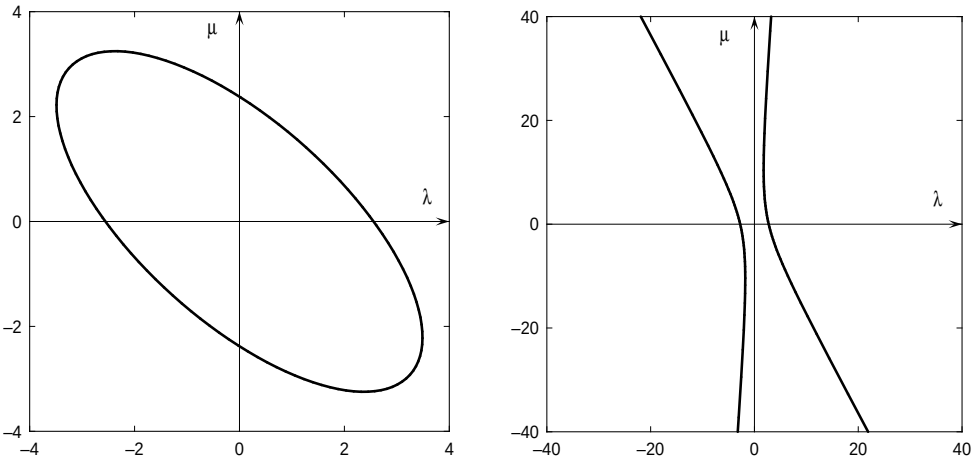

Figure 4: The locus of solutions to equation (16) in the (λ, μ) plane, defined by equations (17)–(18) and (19)–(20) when $s = +1$ and $s = -1$, respectively.

Once the complex values $\mathbf{w}_0, \mathbf{w}_1, \mathbf{w}_2, \mathbf{w}_3$ are computed from (14)–(15) and (17)–(18) or (19)–(20), the Bézier control points of the G^2 degree 7 PH corner

curve may be constructed from them through the expressions

$$\begin{aligned}
\mathbf{p}_1 &= \mathbf{p}_0 + \frac{1}{7}\,\mathbf{w}_0^2\,, \\
\mathbf{p}_2 &= \mathbf{p}_1 + \frac{1}{7}\,\mathbf{w}_0\mathbf{w}_1\,, \\
\mathbf{p}_3 &= \mathbf{p}_2 + \frac{1}{7}\,\frac{3\,\mathbf{w}_1^2 + 2\,\mathbf{w}_0\mathbf{w}_2}{5}\,, \\
\mathbf{p}_4 &= \mathbf{p}_3 + \frac{1}{7}\,\frac{\mathbf{w}_0\mathbf{w}_3 + 9\,\mathbf{w}_1\mathbf{w}_2}{10}\,, \\
\mathbf{p}_5 &= \mathbf{p}_4 + \frac{1}{7}\,\frac{3\,\mathbf{w}_2^2 + 2\,\mathbf{w}_1\mathbf{w}_3}{5}\,, \\
\mathbf{p}_6 &= \mathbf{p}_5 + \frac{1}{7}\,\mathbf{w}_2\mathbf{w}_3\,, \\
\mathbf{p}_7 &= \mathbf{p}_6 + \frac{1}{7}\,\mathbf{w}_3^2\,.
\end{aligned}$$

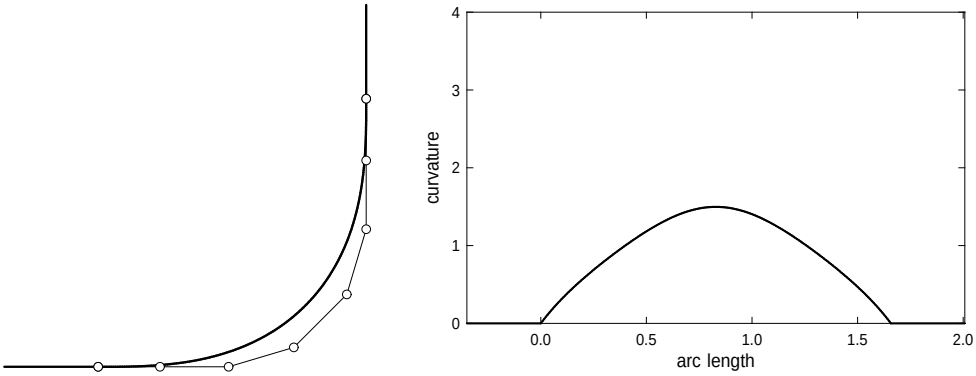

Figure 5: Left: canonical degree 7 G^2 PH corner curve for $\phi = \frac{1}{2}\pi$, with its Bézier control polygon. Right: curvature profile of this G^2 PH corner curve.

It is found that the shape of the degree 7 PH corner defined by (14)–(15) and (17)–(18) is sensitive to the choice of the ϕ parameter, with acceptable shapes resulting from a relatively narrow range about $\phi = \frac{1}{2}\pi$. Figure 5 shows the corner shape and its curvature profile for the specific case $\phi = \frac{1}{2}\pi$. The curve compares favorably with the unique G^1 PH cubic and G^2 PH quintic corners shown in Figures 1 and Figure 3. Unlike the former, it is curvature–continuous and does not closely resemble a circular arc. Also, the extremum

curvature is only ~ 1.4974, as compared to ~ 3.8378 for the latter. The three corner shapes, and their curvatures versus fractional arc length (the total arc lengths are somewhat different), are compared in Figure 6.

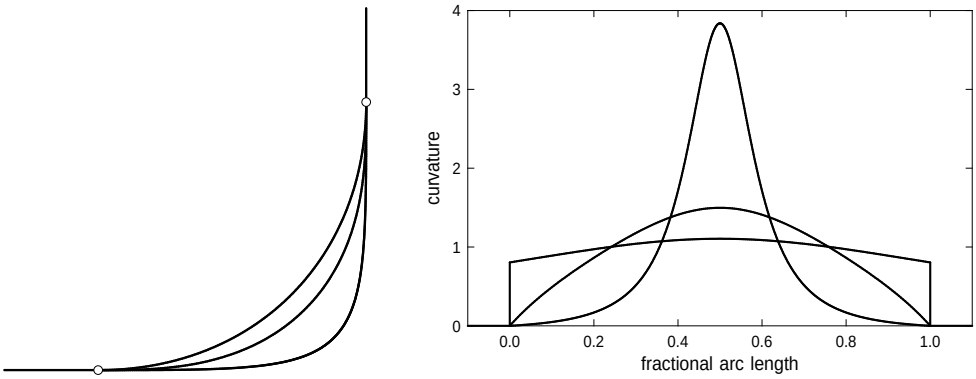

Figure 6: Left: comparison of G^1 PH cubic, G^2 PH quintic, and G^2 degree 7 PH corners. Right: curvature profiles, as functions of fractional arc length.

As a further shape comparison of the G^1 PH cubic, G^2 PH quintic, and G^2 degree 7 PH corner with $\phi = \frac{1}{2}\pi$, Figure 7 shows each of these curve together with its evolute (locus of centers of curvature) and circle of curvature at the vertex (point of extremum curvature) of the corner curve. Note that the cusp of the evolute corresponds to the center of curvature at the vertex.

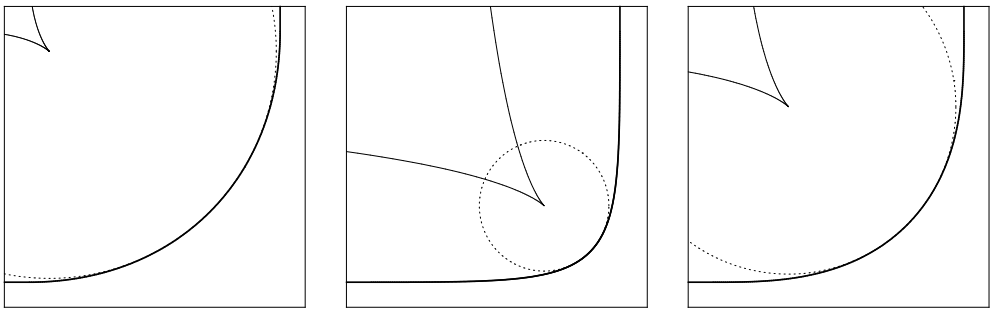

Figure 7: The evolutes and smallest circles of curvature for the G^1 PH cubic (left), G^2 PH quintic (center), and degree 7 G^2 PH corner (right) with $\phi = \frac{1}{2}\pi$.

Figure 8 illustrates the effect[3] of varying ϕ away from $\frac{1}{2}\pi$. As ϕ is reduced below $\frac{1}{2}\pi$, one obtains a sharper corner, with a more pronounced mid–point curvature extremum, but for ϕ less than $\sim 0.36\,\pi$ the corner develops slight negative curvatures and a severe curvature extremum. As ϕ increases above $\frac{1}{2}\pi$, on the other hand, the corner becomes much shallower. When $\phi \approx 0.53\pi$, one obtains a quite remarkable curvature distribution — nearly constant over most of the curve, with a rapid rise and fall near the end points. As observed in Figure 8, the curvature profile exhibits an increasingly pronounced bimodal distribution as ϕ increases above $\sim 0.53\pi$. Figure 9 illustrates the variation of the maximum (mid–point) curvature for $0.36\,\pi \leq \phi \leq 0.53\,\pi$.

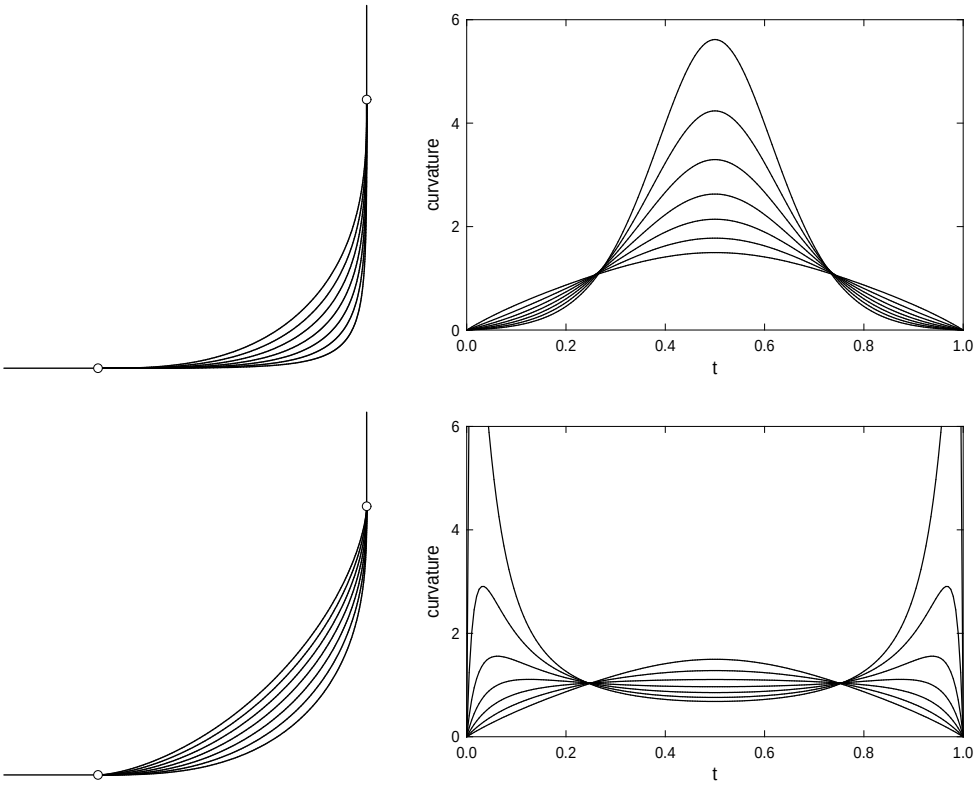

Figure 8: G^2 PH corner curves of degree 7, with their curvature profiles, for the parameter ranges $0.4\pi \leq \phi \leq 0.5\pi$ (upper) and $0.5\pi \leq \phi \leq 0.6\pi$ (lower).

[3]Since the total arc length of the corner curves varies with ϕ, the curvature profiles are plotted as functions of the curve parameter t, rather than arc length, in Figure 8.

Experiments show that values of ϕ outside the interval $[\,0.36\,\pi, 0.53\,\pi\,]$ typically produce curves of poor shape, with tight loops, negative curvature, or a bimodal curvature profile, and should therefore be avoided. In practice, the range $0.36\,\pi \le \phi \le 0.53\,\pi$ offers considerable freedom in manipulating the corner shape, while ensuring (i) a unimodal curvature distribution; (ii) a reasonable curvature extremum; and (iii) absence of negative curvature and loops. As a default, the case $\phi = \frac{1}{2}\pi$ is an excellent choice (see Figure 5).

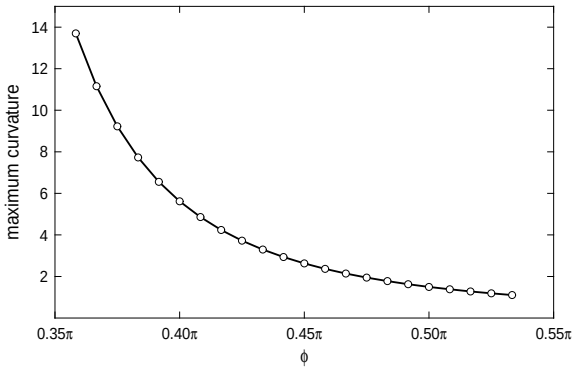

Figure 9: Variation of the maximum curvature with the parameter ϕ for the degree 7 G^2 PH corner defined by (14), (15), and (17)–(18) with $p = q = 1$.

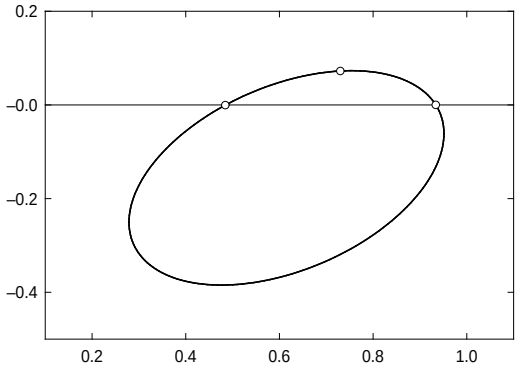

Figure 10: The control point $\mathbf{p}_3$ traces an ellipse as ϕ varies, with only the portion between $\phi \approx 0.36\,\pi$ (on the right) and $\phi \approx 0.62\,\pi$ (on the left) lying above the x–axis. The location of $\mathbf{p}_3$ for the value $\phi = \frac{1}{2}\,\pi$ is also shown.

Figure 10 shows that the locus traced by the control point $\mathbf{p}_3$, as ϕ varies, is an ellipse. It is observed that $\mathbf{p}_3$ lies above the x–axis — ensuring positive curvature — only for $0.36\,\pi \lesssim \phi \lesssim 0.62\,\pi$. The highest location of $\mathbf{p}_3$ above the x–axis occurs for ϕ slightly less than $\frac{1}{2}\,\pi$ — namely, $\phi \approx 0.49\,\pi$.

Although they are formal solutions to the given boundary conditions, the G^2 interpolants to the corner data defined by (14)–(15) with $p = q = -1$, in conjunction with expressions (19)–(20), were found to be of unacceptable shape — with negative curvature and/or small or large loops — for all values of the parameter ϕ. These solutions should therefore be discounted.

6 Spliced G^2 PH quintic corner

It has been seen that the PH cubics and PH quintics define unique G^1 and G^2 corners, respectively, while degree 7 PH curves admit G^2 corners embody a single free parameter, that proves useful in tuning the curvature profile. As a final corner shape, incorporating two degrees of freedom, we consider here a solution based on splicing together two PH quintic segments.

Consider two PH quintic segments $\mathbf{r}_1(\xi)$ and $\mathbf{r}_2(\xi)$, such that $\mathbf{r}_1(0) = (0,0)$, $\mathbf{r}_1(1) = \mathbf{r}_2(0)$, $\mathbf{r}_2(1) = (1,1)$. By symmetry, the juncture point must have coordinates $\mathbf{r}_1(1) = \mathbf{r}_2(0) = (\alpha, 1-\alpha)$ with $0 < \alpha < 1$. At that point, the two curves must also have a common tangent (inclined at angle $\frac{1}{4}\pi$ with the positive x–direction), and equal curvatures, to ensure a G^2 splice.

In fact, $\mathbf{r}_2(\xi)$ must be a reflection of $\mathbf{r}_1(\xi)$ in the diagonal line between $(0,0)$ to $(1,1)$, so we can focus on the construction of $\mathbf{r}_1(\xi)$. Specfiying $\mathbf{r}_1(\xi)$ in the complex representation by substituting (6) into (3) and integrating, it must satisfy the interpolation constraints

$$\mathbf{r}_1(0) = 0\,, \quad \mathbf{r}_1'(0) = \lambda^2\,, \quad \kappa(0) = 0\,,$$

and

$$\mathbf{r}_1(1) = \alpha + \mathrm{i}\,(1-\alpha)\,, \quad \mathbf{r}_1'(1) = \mu^2 \exp(\mathrm{i}\tfrac{1}{4}\pi)$$

with $\lambda \neq 0$, $\mu \neq 0$, and $0 < \alpha < 1$. The condition $\mathbf{r}_1(0) = 0$ is achieved by choice of the integration constant upon integrating (3), and $\mathbf{r}'(0) = \lambda^2$ yields $\mathbf{w}_0 = \lambda$, where we again assume $\lambda > 0$ without loss of generality. Also, the condition $\kappa(0) = 0$ becomes $\mathrm{Im}(\lambda(u_1 + \mathrm{i}\,v_1)) = 0$, so $v_1 = 0$ since $\lambda \neq 0$, and hence $\mathbf{w}_1 = u_1$. Finally, from $\mathbf{r}'(1) = \mu^2 \exp(\mathrm{i}\frac{1}{4}\pi)$ we have $\mathbf{w}_2 = \pm\mu \exp(\mathrm{i}\frac{1}{8}\pi)$.

These expressions for $\mathbf{w}_0, \mathbf{w}_1, \mathbf{w}_2$ must satisfy the end–point condition $\mathbf{r}(1) = \alpha + (1-\alpha)\mathrm{i}$, which may be expressed as

$$\frac{1}{5}\left[\mathbf{w}_0^2 + \mathbf{w}_0\mathbf{w}_1 + \frac{2\mathbf{w}_1^2 + \mathbf{w}_0\mathbf{w}_2}{3} + \mathbf{w}_1\mathbf{w}_2 + \mathbf{w}_2^2\right] \;=\; \alpha + (1-\alpha)\,\mathrm{i}\,.$$

Substituting for $\mathbf{w}_0, \mathbf{w}_1, \mathbf{w}_2$ and taking real and imaginary parts, this becomes

$$2u_1^2 + 3(\lambda \pm \mu\cos\tfrac{1}{8}\pi)\,u_1 + 3\lambda^2 \pm \lambda\mu\cos\tfrac{1}{8}\pi + 3\mu^2\cos\tfrac{1}{4}\pi \;=\; 15\,\alpha\,, \qquad (21)$$

$$\pm 3\mu\sin\tfrac{1}{8}\pi\,u_1 \pm \lambda\mu\sin\tfrac{1}{8}\pi + 3\mu^2\sin\tfrac{1}{4}\pi \;=\; 15(1-\alpha)\,. \qquad (22)$$

Since these two real equations incorporate the four free parameters $\alpha, \lambda, \mu, u_1$ we may expect the solutions to exhibit two degrees of freedom. Eliminating α between (21) and (22) yields a quadratic equation

$$a_2 u_1^2 + a_1 u_1 + a_0 \;=\; 0 \qquad (23)$$

in u_1 with coefficients dependent on λ and μ, namely

$$a_2 \;=\; 2\,, \quad a_1 \;=\; 3(\lambda \pm \mu(\sin\tfrac{1}{8}\pi + \cos\tfrac{1}{8}\pi))\,,$$

$$a_0 \;=\; 3\lambda^2 \pm \lambda\mu(\sin\tfrac{1}{8}\pi + \cos\tfrac{1}{8}\pi) + 3\mu^2(\sin\tfrac{1}{4}\pi + \cos\tfrac{1}{4}\pi) - 15\,.$$

Note that the discriminant $\Delta = a_1^2 - 4a_0a_2$ of (23) can be expressed as

$$\Delta \;=\; 120 - 15\lambda^2 \pm 10(\sin\tfrac{1}{8}\pi + \cos\tfrac{1}{8}\pi)\lambda\mu + (9 - 15\sin\tfrac{1}{4}\pi - 24\cos\tfrac{1}{4}\pi)\mu^2\,,$$

and we must have $\Delta \geq 0$ to obtain a real u_1 value. If the + sign is chosen, this condition identifies the set of feasible values as the interior of an ellipse centered on the origin in the (λ, μ) plane. Choosing feasible λ and μ values, one can solve (23) for u_1 and obtain α from (21) — the complex coefficients $\mathbf{w}_0, \mathbf{w}_1, \mathbf{w}_2$ in (6) are then completely determined.

Once the control points for the first segment of the spliced G^2 PH quintic corner are computed from (7) using $\mathbf{p}_0 = 0$ and these $\mathbf{w}_0, \mathbf{w}_1, \mathbf{w}_2$ values, the control points for the second segment can be determined from (7) using $\mathbf{p}_0 = \alpha + (1-\alpha)\mathrm{i}$ and $\mathbf{w}_0, \mathbf{w}_1, \mathbf{w}_2$ values obtained by applying the transformation

$$\mathbf{w}_k \;\rightarrow\; \frac{1+\mathrm{i}}{\sqrt{2}}\,\overline{\mathbf{w}}_{k-2}\,, \quad k = 0, 1, 2$$

to the values for the first segment — this transformation allows for the fact $\mathbf{r}_2(\xi)$ is the mirror image of $\mathbf{r}_1(\xi)$ in the diagonal line from $(0, 1)$ to $(1, 0)$.

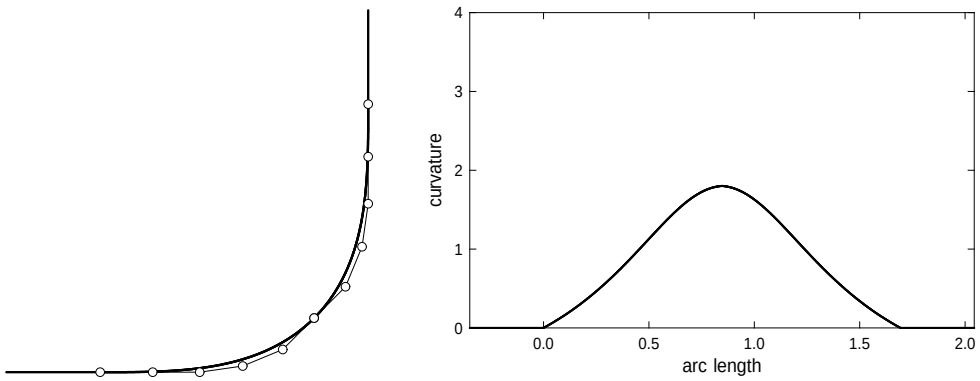

Figure 11: Left: spliced G^2 PH quintic corner curve defined by the parameter values $(\lambda, \mu) = (0.99, 0.91)$. Right: the corresponding curvature distribution.

The parameter values $(\lambda, \mu) = (0.99, 0.91)$ were found empirically to yield an excellent spliced G^2 PH quintic corner shape when the + sign is used in (21)–(22). The curve, together with its control polygon and curvature profile, are illustrated in Figure 11. The extremum curvature, at the juncture of the two segments, is ~ 1.8013 — slightly higher than for the degree 7 G^2 corner with $\phi = \frac{1}{2}\pi$, but much lower than for that defined by a single PH quintic.

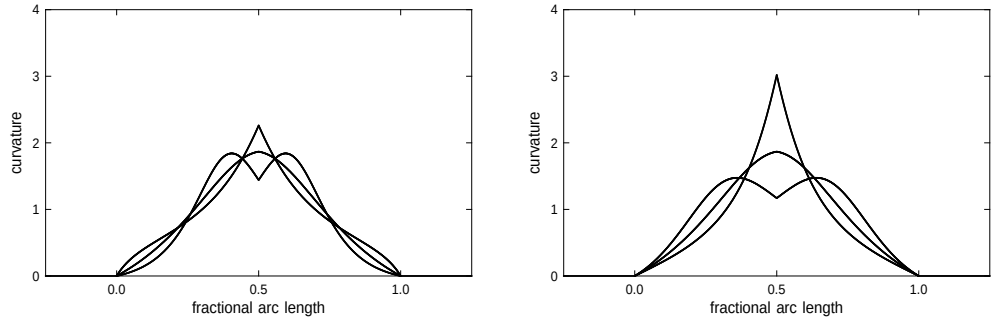

Figure 12: Dependence of the curvature profiles for the G^2 spliced PH quintic corner on the λ and μ parameters — left: for the values $\lambda = 0.8, 1.0, 1.2$ with μ fixed at 0.9; and right: for the values $\mu = 0.8, 0.9, 1.0$ with λ fixed at 1.0.

Figure 12 illustrates the influence of the λ and μ parameters on the corner curvature profile. If either parameter is reduced below the nominal value, the extremum curvature increases. If either is increased above the nominal value,

the curvature profile assumes a bimodal configuration. These effects are more pronounced with variation of the μ parameter than with the λ parameter.[4]

A systematic shape optimization of the spliced G^2 PH quintic corner with respect to the (λ, μ) parameters is a non–trivial task, that we do not attempt here. It should be noted that these parameters can also be exploited in other ways — for example, a G^3 splice can be achieved by requiring that $\kappa'(1) = 0$. From (4) the derivative of the curvature can be expressed as

$$\kappa' \;=\; \frac{2\,|\mathbf{w}|^2 \mathrm{Im}(\overline{\mathbf{w}}\mathbf{w}'') \;-\; 8\,\mathrm{Re}(\overline{\mathbf{w}}\mathbf{w}')\,\mathrm{Im}(\overline{\mathbf{w}}\mathbf{w}')}{|\mathbf{w}|^6}\,,$$

and substituting (6) with the above expressions for $\mathbf{w}_0, \mathbf{w}_1, \mathbf{w}_2$ the condition $\kappa'(1) = 0$ reduces to

$$8\cos\tfrac{1}{8}\pi\, u_1^2 \;\mp\; 6\,\mu\, u_1 \;\mp\; \lambda\mu \;=\; 0\,. \tag{24}$$

Equations (23) and (24) must have a common root, i.e., their resultant with respect to u_1 must vanish. This imposes a constraint between λ and μ, leaving just one freedom (there are insufficient freedoms to ensure G^3 continuity at the splice point *and* the connections with the linear segments).

7 Closure

Several solutions to the problem of specifying rounded right–angle corners in terms of G^2 planar Pythagorean–hodograph curves have been presented. The simplest consists of a (unique) single PH quintic segment — in this case, the extremum curvature is relatively large, but the corner shape is nevertheless aesthetically quite attractive. The G^2 corners defined by a single PH curve of degree 7 comprise a one–parameter family, offering scope for adjustment of the curvature distribution. A nominal value for this parameter was identified, that generates an appealing corner shape with a smooth unimodal curvature distribution, and a modest extremum curvature. Finally, a G^2 corner based on splicing together two PH quintics was proposed, with two free parameters for shape adjustment. Nominal values for the parameters were identified, and their influence on the curvature profile was studied.

[4] It is also possible to study the dependence of the location of control point $\mathbf{p}_3$ on the parameters λ, μ (as with the degree 7 case in Section 5), but the analysis is more involved because of the two degrees of freedom and the intermediate quadratic equation (23).

The G^2 corner constructions can be easily implemented using the complex representation of planar PH curve, and incur little more than the solutions of quadratic equations. It should be noted that sign ambiguities arise at various points in the solution procedure, and inappropriate choices can yield curves with unacceptable shape properties (negative curvature or tight loops) that nevertheless satisfy the specified boundary conditions. The appropriate signs, and ranges for the free parameters, are indicated throughout the presentation to ensure that such undesired extraneous solutions are circumvented.

The design of G^2 corners in terms of PH curves offers several important advantages over "ordinary" polynomial or spline curves, including exact arc length measurement, rational offset curves, and the availability of real–time interpolator algorithms to drive CNC machines directly from the analytic curve description for manufacturing or inspection applications.

Acknowledgement

The author is grateful to one referee for detailed comments and suggestions.

References

[1] K. G. Baass (1984), The use of clothoid templates in highway design, *Transport. Forum* **1**, 47–52.

[2] R. T. Farouki (1994), The conformal map $z \rightarrow z^2$ of the hodograph plane, *Comput. Aided Geom. Design* **11**, 363–390.

[3] R. T. Farouki (1997), Pythagorean–hodograph quintic transition curves of monotone curvature, *Comput. Aided Design* **29**, 601–606.

[4] R. T. Farouki (2008), *Pythagorean–Hodograph Curves: Algebra and Geometry Inseparable*, Springer, Berlin.

[5] R. T. Farouki and T. Sakkalis (1990), Pythagorean hodographs, *IBM J. Res. Develop.* **34**, 736–752.

[6] Z. Habib and M. Sakai (2007), G^2 Pythagorean hodograph quintic transition between two circles with shape control, *Comput. Aided Geom. Design* **24**, 252–266.

[7] Z. Habib and M. Sakai (2009), G^2 cubic transition between two circles with shape control, *J. Comput. Appl. Math.* **223**, 133–144.

[8] Z. Habib and M. Sakai (2010), Admissible regions for rational cubic spirals matching G^2 Hermite data, *Comput. Aided Design* **42**, 1117–1124.

[9] Z. Habib and M. Sakai (2011), Cubic spiral transition matching G^2 Hermite end conditions, *Numer. Math. Theor. Meth. Appl.* **4**, 525–536.

[10] Z. Habib and M. Sakai (2012), Fairing arc spline and designing by using cubic Bézier spiral segments, *Math. Model. Anal.* **17**, 141–160.

[11] P. Hartman (1957), The highway spiral for combining curves of different radii, *Trans. Amer. Soc. Civil Eng.* **22**, 389–409.

[12] D. S. Meek and D. J. Walton (1992), Clothoid spline transition spirals, *Math. Comp.* **59**, 117–133.

[13] D. J. Walton and D. S. Meek (1996), A planar cubic Bézier spiral, *J. Comput. Appl. Math.* **72**, 85–100.

[14] D. J. Walton and D. S. Meek (1996), A Pythagorean–hodograph quintic spiral, *Comput. Aided Design* **28**, 943–950.

[15] D. J. Walton and D. S. Meek (1998), G^2 curves composed of planar cubic and Pythagorean–hodograph spirals, *Comput. Aided Geom. Design* **15**, 547–566.

[16] D. J. Walton and D. S. Meek (2002), Planar G^2 transition with a fair Pythagorean hodograph quintic curve, *J. Comput. Appl. Math.* **138**, 109–126.

[17] D. J. Walton and D. S. Meek (2004), A generalisation of the Pythagorean hodograph quintic spiral, *J. Comput. Appl. Math.* **172**, 271–287.

[18] D. J. Walton and D. S. Meek (2007), G^2 curve design with a pair of Pythagorean–hodograph quintic spiral segments, *Comput. Aided Geom. Design* **24**, 267–285.

[19] D. J. Walton and D. S. Meek (2009), G^2 blends of linear segments with cubics and Pythagorean–hodograph quintics, *Int. J. Comput. Math.* **86**, 1498–1511.

[20] D. J. Walton and D. S. Meek (2013), Curve design with more general planar Pythagorean–hodograph quintic spiral segments, *Comput. Aided Geom. Design* **30**, 707–721.